CrossMark

Structure and piezoelectric properties of $K_{0.5}Na_{0.5}NbO_3$ based lead-free piezoceramics with slight deviation from A-site K or Na stoichiometry

Qing Ma[1] · Bingbing Wan[2] · Lijin Cheng[2] · Shaojun Liu[2] · Fusheng Liu[3]

Abstract The dependence of structure and piezoelectric response d_{33} on individual excess A-site K or Na in $K_{0.5}Na_{0.5}NbO_3$ based lead-free piezoceramics is reported. The coexistence of orthorhombic, tetragonal, and monoclinic phases at room temperature is observed in the investigated $0.94K_{0.5+x}Na_{0.5}NbO_3$–$0.06LiNbO_3$ and $0.94K_{0.5}Na_{0.5+y}NbO_3$–$0.06LiNbO_3$ ceramics (x, y = 0–0.025). The weight ratio of three phases, orthorhombic-tetragonal phase transition temperature, and d_{33} value are highly sensitive to A-site K or Na nonstoichiometry. A-site Na nonstiochiometry plays a dominant role in enhancing the electrical properties of KNN by significantly reducing the weight ratio percentage of monoclinic phase and shifting the orthorhombic-tetragonal phase transition temperature to lower temperatures.

Keywords Piezoceramics · Lead-free · Non-stoichiometry

✉ Shaojun Liu
liumatthew@csu.edu.cn

✉ Fusheng Liu
fsliu@szu.edu.cn

[1] Key Laboratory of Low-carbon Energy and Energy-saving Technology, Research Institute of Tsinghua University in Shenzhen, Shenzhen 518057, China

[2] State Key Laboratory for Powder Metallurgy, Central South University, Changsha 410083, China

[3] School of Materials Science and Engineering, Shenzhen University, Shenzhen 510085, China

1 Introduction

Innovations in actuators, sensors, and ultrasonic transducers have been the driving force for the development of piezoelectric ceramics [1]. Due to their high piezoelectric response, large scale production capability and the tailoring of their properties through composition, lead zirconate-titanate ceramics (PZT) are the most widely used piezoelectrics [2, 3]. However, the lead-based PZT piezoelectrics contain more than 60 wt% toxic lead, leading to a various environmental problems [4]. One widely investigated alternative is based on potassium sodium niobate solid solutions [5, 6]. For example, $K_{0.5}Na_{0.5}NbO_3$ (KNN) based piezoelectrics with relatively high piezoelectric constant and phase transition temperature are attracting more attention and emerging as a promising lead free piezoelectrics candidate [7–11]. Unlike the lead based PZT piezoelectrics, enhanced properties of KNN based lead-free ceramics are usually due to the shift of the orthorhombic-tetragonal phase transition temperature (OT-PTT) that is compositional dependence to near room temperature [12]. Guo et.al reported significantly enhanced piezoelectric properties for KNN based ceramics with the composition near the OT-PTT region by doping $LiNbO_3$ [13].

However, Na and K evaporate unavoidably during the elevated temperature sintering. This can result in the formation of secondary phases and the nonstoichiometry of KNN [14, 15]. Additionally, KNN based piezoelectrics could be easily off stoichiometric from the beginning unless properly handled since alkali metal carbonates, such as Na_2CO_3 or K_2CO_3, are hygroscopic. While the influence of volatilization on the dielectric properties has been widely studied in Pb-based perovskite systems [16], investigations also indicate that volatile elements have distinct effect on the microstructure and properties of lead-free piezoelectric [17].

In particular, the difference in evaporation rate between A-site K and Na and induced point defects by nonstoichiometry make the analysis of relationship between structure and properties of KNN ceramics more complex. Several reports confirmed that it is of significant importance to adjust K/Na ratio and sintering temperature and A-site alkali excess amount to obtain enhanced dielectric and piezoelectric properties [18–20]. Zhang et.al predicted [21] that a large change in the structure over a small compositional change for $K_{0.3}Na_{0.7}NbO_3$ could potentially result in enhanced physical properties based on the study of crystallographic structures of KNN based ceramics. Our recent study showed that A-site (K + Na) nonstoichiometry plays a key role in enhancing piezoelectric response by shifting the OT-PTT to lower temperatures [22]. However, it is not clear what the role of individual A-site K or Na nonstoichiometry plays in shifting the OT-PTT and affecting the electrical properties of KNN based ceramics.

In the present study, the dependence of phase structure and electrical properties on individual excess A-site K or Na in $0.94K_{0.5+x}Na_{0.5}NbO_3$–$0.06LiNbO_3$ (K_xNLN) with x = 0 ~ 0.025 and $0.94K_{0.5}Na_{0.5+y}NbO_3$–$0.06LiNbO_3$ (KN_yLN) with y = 0 ~ 0.025 was investigated. The coexistence of orthorhombic, tetragonal, and monoclinic phases was observed at room temperature.

2 Experimental

All ceramics were prepared by a conventional solid-state reaction method. Raw materials were sodium carbonate (Na_2CO_3, 99.8 %), potassium carbonate (K_2CO_3, 99 %), lithium carbonate (Li_2CO_3, 99.99 %), and niobium oxide (Nb_2O_5, 99.5 %). Since the changes in composition in the investigated samples were so small that several precautions were taken to make a series of non-stoichiometric samples. We dried all the powders in a vacuum dry oven to avoid possible water absorption by powders. Immediately, we used large batches of powders (60 g) and weighed it out using an analytic balance with a high precision (0.0001 g) to meet such tolerances and convinced that the actual compositions consistently followed the nominal compositions. Raw powders were wet-milled by mixing a certain amount of raw materials and ZrO_2 milling balls for 24 h. After calcination at 750 °C for 3 h, the powders were ball milled and then pressed into disk samples, followed by sintering at 1080 °C for 3 h in air. The samples were poled in 130 °C silicon oil by applying a 30 kV/cm DC electric field for 30 min.

X-ray diffraction characterization was performed using Cu K_{α} radiation (λ = 1.54178 Å) in θ-2θ mode (D/max 2500PC, Rigaku, Japan). Scans were taken in a 2θ range from 20 to 80° with a step size of 0.02° and accumulation time

40 min. Due to the heavy overlapping of the peaks of these two phases (see the inset of Fig. 1(a)), the XRD patterns of K_xNLN ceramics between 2θ = 44° and 47° with a step size of 0.01° were further recorded with a Panalytical Xpert Pro MPD diffractometer using only $CuK_{\alpha1}$ radiation. Rietveld refinement analysis using TOPAS software was carried out to further identify the unknown phase. All the samples used in XRD are as-synthesized powders by solid state reaction or crushed and ground powders.

The Raman spectra were measured by Renishaw Micro-Raman Spectroscopy System (Renishaw InVia Reflex). Using 514.5 nm Ar^+ blue laser as exciting source, the Raman Spectroscopy scanned the region on the surface of pellets with ~2–3 μm in diameter on the range of wave number from 1000 cm^{-1} to 100 cm^{-1}. The microstructure and morphology was characterized by a field emission scanning electron microscopy (FE-SEM, Hitachi S-4700). The temperature dependence of dielectric constant (ε_r) and loss tangent (tanδ) was measured by LCR meter (E4980A, Aglient). The piezoelectric constant d_{33} was measured using a quasi-static d_{33} meter (Model ZJ-6 A, Institute of Acoustics Academic Sinica).
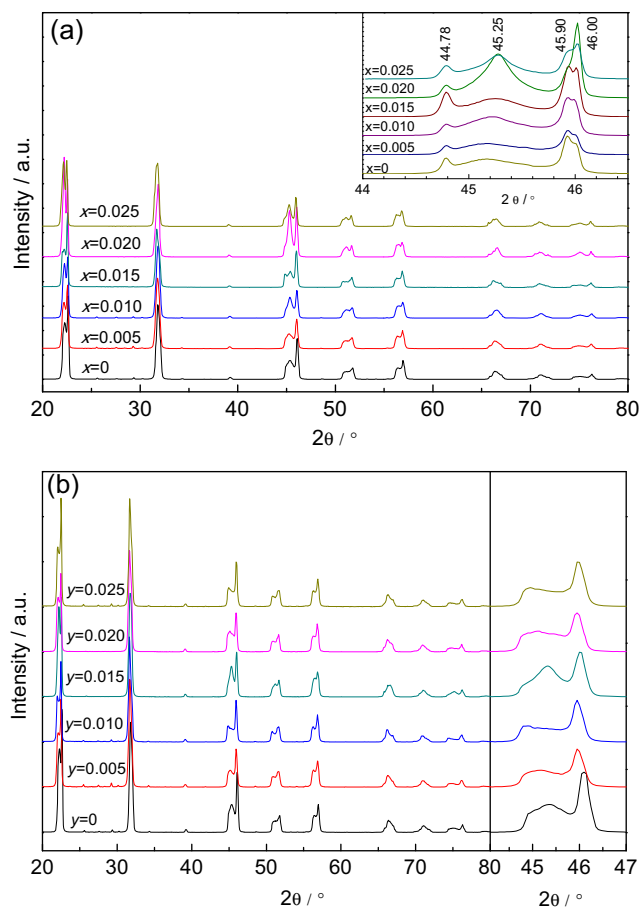
Fig. 1 XRD patterns of **(a)** K_xNLN and **(b)** KN_yLN ceramics with x = 0–0.025 and y = 0–0.025. Note: Only the K_xNN series was investigated with only $CuK\alpha_1$
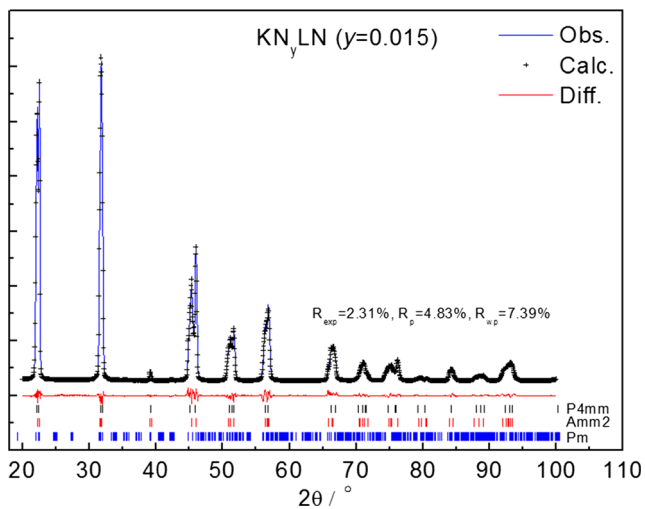
Fig. 2 The Rietveld refinement of XRD patterns of KN$_y$LN (y = 0.015) ceramics

3 Results and discussion

The XRD patterns for K$_x$NLN (x = 0 ~ 0.025) and KN$_y$LN (y = 0 ~ 0.025) ceramics are shown in Fig. 1(a) and (b), respectively. Two common phases in KNN based piezoelectrics, the orthorhombic and tetragonal, can be easily identified in all the investigated samples. Several very weak peaks can

be occasionally observed between 2θ = 25° and 30° only in KN$_y$LN (y = 0.005), which is usually associated to the existence of secondary phases with tungsten bronze structure due to the volatilization of alkaline elements [23]. However, the perovskite structures were formed in all the other investigated compositions. Due to the heavy overlapping of the peaks of these two phases, the XRD patterns of K$_x$NLN ceramics between 2θ = 44° and 47° were further recorded with a Panalytical Xpert Pro MPD diffractometer using only CuK$_{\alpha 1}$ radiation, as shown in the inset of Fig. 1(a). It is clearly seen from the inset that there are four peaks centered at ~44.78, ~45.25, ~45.90, and ~46.00° in all the samples, respectively. Especially, the peak at 2θ = 45.25° is very broad and obviously overlaps the peak of an unknown third phase. Given the appearance of the broad peak in all ceramics, the contribution of impurity phase to broad peaks can be ruled out.

Rietveld refinement analysis was carried out to identify the unknown phase in the XRD patterns. As shown in Fig. 2, good reliable factors are achieved for the Rietveld refinement of the XRD patterns when the unknown structure is assigned to monoclinic phase. The reliable factors of R_{exp}, R_p and R_{wp} of KNLN are derived to be 3 ~ 4, 4.8 ~ 6.8 and 7.1 ~ 8.7 %, respectively. R_{exp} is an indicator of original measured XRD data and the limit of R_{wp} reliable factor, respectively. In contrast, R_p indicates the reliability fitting the XRD patterns. R_{wp} is the weighted average
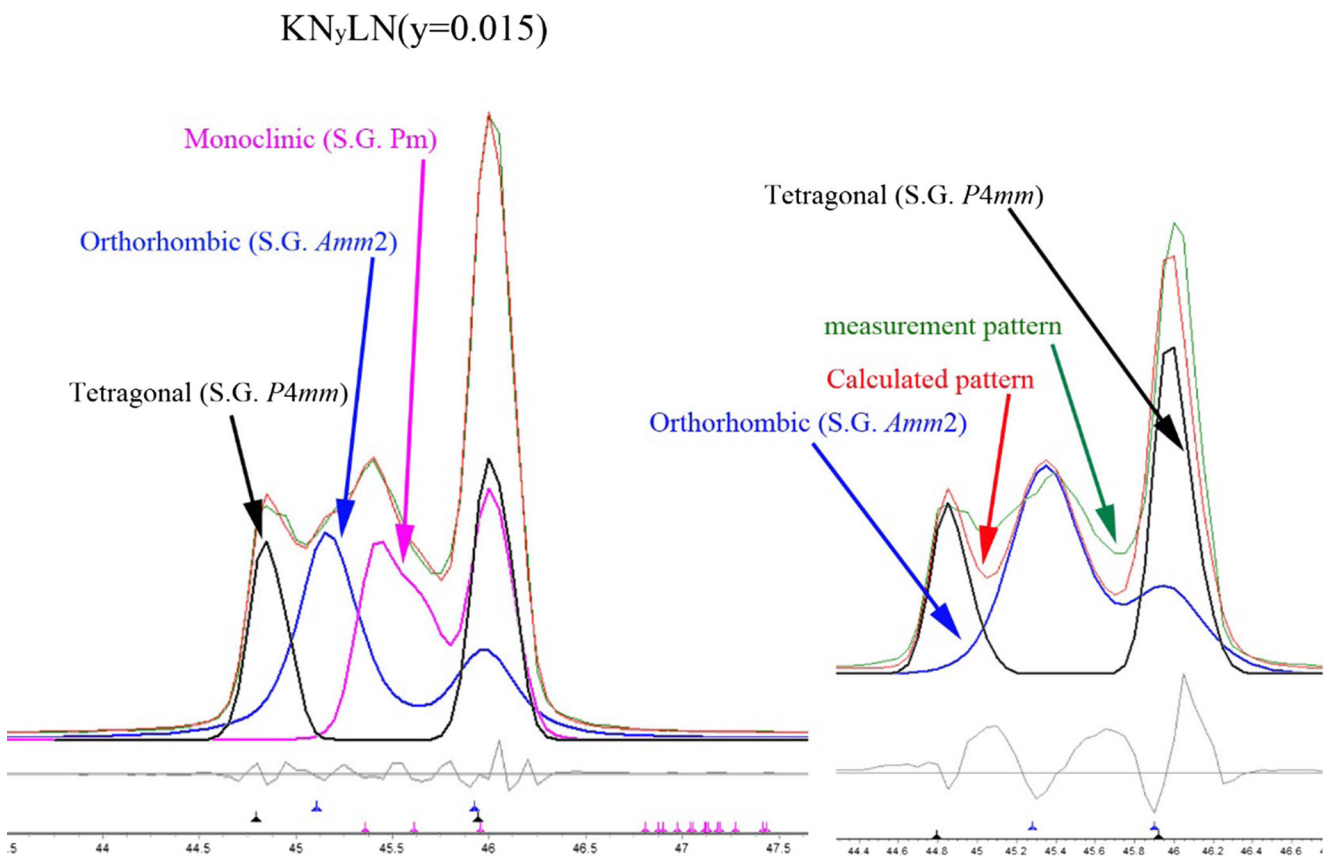
Fig. 3 The Rietveld refinement analysis results of KN$_y$LN (y = 0.015) ceramics for the three-phase refinement (**a**) and the two-phase refinement (**b**)

Table 1 Dielectric properties and d_{33} of K_xNLN and KN_yLN with x, y = 0–0.025

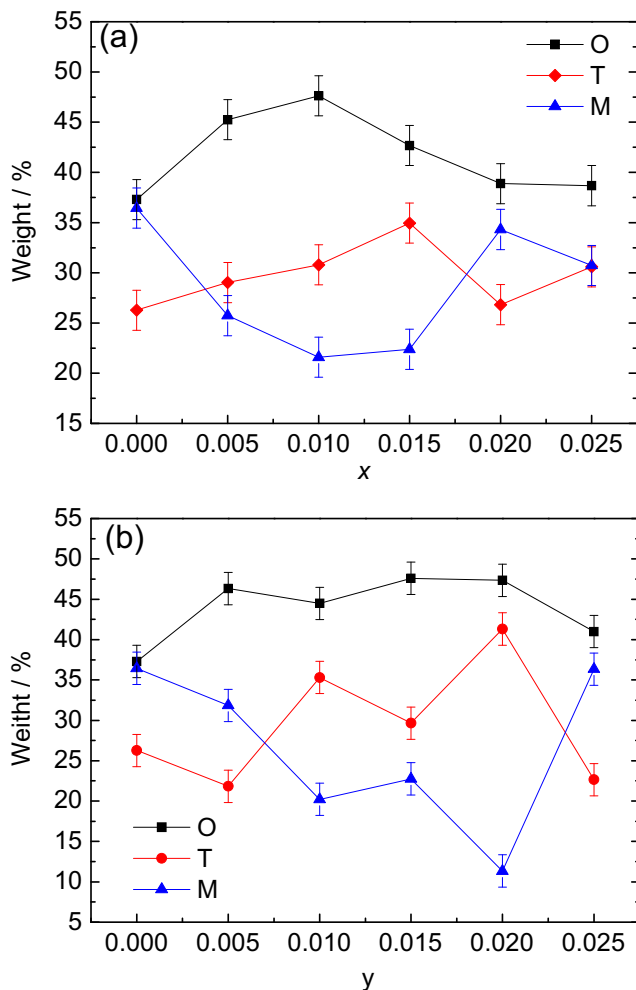| K_xNN/KN_yN	x, y = 0	x = 0.005	x = 0.010	x = 0.015	x = 0.020	x = 0.025	y = 0.005	y = 0.010	y = 0.015	y = 0.020	y = 0.025
ε_r	498.3	395.3	717.1	519.5	474.8	403.2	493.2	645.8	608.6	605	570.3
tanδ	0.0441	0.0988	0.0305	0.1445	0.153	0.0565	0.1643	0.1752	0.1512	0.1408	0.3168
T_c (°C)	419	420	428	423	421	408	416	425	428	426	427
T_{O-T} (°C)	69	91	40	52	92	116	91	71	56	42	39
d_{33} (pC/N)	116	112	116	128	126	109	112	138	134	167	147

of R_p reliable factor. G_{of} factor denotes R_{wp}/R_{exp}. Usually, these derived results are considered to be reliable if the value of G_{of} and R_{wp} is below 2 and 10 %, respectively. We would like to mention that given the weak intensity of diffraction background peaks, the reliability of data listed in Table 2 can be very high.

It is well known that the Rietveld refinement analysis calculates the relative intensities of the XRD diffraction peaks based on the structural model of phases by adjusting the scale factor S to match the measured diffraction peaks' intensity. By refining the preferred orientation and atomic positions of

Table 2 The calculated lattice constants of K_xNLN and KN_yLN

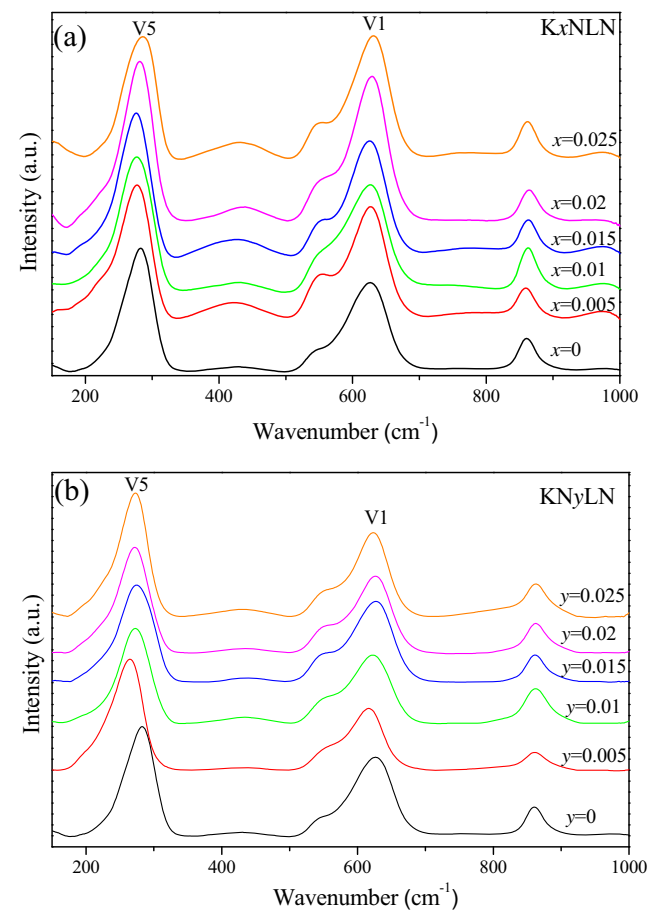| Sample	Phase Name	a (Å)	b (Å)	c (Å)	beta(°)	Weight percent (%)
K_xN_yLN x, y = 0	Orthorhombic	3.944(1)	5.675(1)	5.677(1)		37.29(2)
	Tetragonal	3.953(1)		4.038		26.27
	Monoclinic	7.995	7.885	7.959	90.13(3)	36.44
K_xNLN x = 0.005	Orthorhombic	3.942	5.674	5.675		45.25
	Tetragonal	3.954		4.036		29.03
	Monoclinic	7.995	7.885	7.960	90.14	25.73
K_xNLN x = 0.010	Orthorhombic	3.945	5.672	5.663		47.63
	Tetragonal	3.958		4.032		30.79
	Monoclinic	7.989	7.883	7.961	90.12	21.59
K_xNLN x = 0.015	Orthorhombic	3.945	5.675	5.676		42.68
	Tetragonal	3.954		4.041		34.95
	Monoclinic	7.994	7.890	7.962	90.11	22.38
K_xNLN x = 0.020	Orthorhombic	3.946	5.675	5.667		38.88
	Tetragonal	3.964		4.034		26.82
	Monoclinic	7.999	7.885	7.974	90.14	34.31
K_xNLN x = 0.02	Orthorhombic	3.944	5.674	5.669		38.68
	Tetragonal	3.956		4.037		30.59
	Monoclinic	7.996	7.886	7.966	90.11	30.73
KN_yLN y = 0.005	Orthorhombic	3.940	5.675	5.701		46.32
	Tetragonal	3.948		4.040		21.84
	Monoclinic	8.004	7.895	7.955	90.19	31.84
KN_yLN y = 0.010	Orthorhombic	3.943	5.673	5.702		44.48
	Tetragonal	3.948		4.041		35.30
	Monoclinic	8.000	7.889	7.955	90.13	20.22
KN_yLN y = 0.015	Orthorhombic	3.945	5.673	5.667		47.59
	Tetragonal	3.957		4.036		29.66
	Monoclinic	7.992	7.885	7.963	90.11	22.75
KN_yLN y = 0.020	Orthorhombic	3.944	5.675	5.669		47.35
	Tetragonal	3.955		4.036		41.31
	Monoclinic	7.989	7.888	7.959	90.16	11.34
KN_yLN y = 0.025	Orthorhombic	3.939	5.673	5.700		41.00
	Tetragonal	3.947		4.040		22.65
	Monoclinic	8.000	7.893	7.951	90.21	36.34

M (monoclinic) phase, the existence of M phases can be correctly determined. As an example, Fig. 3(a) and (b) show the Rietveld refinement analysis results of KN_yLN (y = 0.015) ceramics for the three-phase and the two-phase refinement, respectively. In addition to O (orthorhombic) and T (tetragonal) phases, the existence of M is clearly observed in the Fig. 3(a). Especially, the R_{wp} factor will be over 15 % if M phase is not considered in the Rietveld refinement. Although TOPAS can not output the data of diffraction peaks if the phases have been refined, all the phases can be indicated by graph as shown in the Fig. 3. It is observed in Fig. 3 that these figures are the results of the screenshot superposition. It is clear that the results of two-phase refinement yield much larger error value than that of three-phase refinement. In a combination with the reliable factors from the Rietveld refinement, it is suggested that the orthorhombic, tetragonal and monoclinic phases coexist in K_xNLN and KN_yLN ceramics with a wide range of A-site K or Na nonstoichiometry at room temperature (Table 1).

Klein et al. [24] predicted that there could be three phase coexistence region of tetragonal (T), Orthorhombic (O) and an unknown "P″" phases in KNN ceramics. A similar third peak, which is featured by humps on the left side of the 020 peak and claimed to be a low temperature (< 0 °C) monoclinic phase, was reported in KNN based ceramics [25]. It should be mentioned that the structure of KNN is complex since it holds an orthorhombic structure. Especially, the perovskite type ABO_3 sub-cell possesses monoclinic symmetry [26]. The uncertainties exist as to the extent of orthorhombic and monoclinic phase fields arising from different octahedral tilt systems [27]. The weight ratio percentages (WRPs) of the three phases in K_xNLN and KN_yLN ceramics derived from the Rietveld refinement are summarized in Table 2 and shown in Fig. 4. It is noticeable that that the WRPs of these phases, especially monoclinic phase, is highly sensitive to a small deviation of A-site Na or K stoichiometry.

While XRD usually gives average structural information, Raman spectroscopy is further used to determine the structure change of these samples. Figure 4(a) and (b) show the Raman spectra of K_xNLN and KN_yLN (x, y = 0, 0.005, 0.01, 0.015, 0.02, and 0.025) between 100 and 1000 cm^{-1} at room temperature, respectively. Two strong peaks at ~625 cm^{-1} (ν_5) and

Fig. 4 Weight ratio percentages of orthorhombic, tetragonal and monoclinic phase in K_xNLN and KN_yLN ceramics with x = 0–0.025 and y = 0–0.025

Fig. 5 Raman spectroscopy of K_xNLN and KN_yLN ceramics with x = 0–0.025 and y = 0–0.025

~265 cm^{-1} (ν_1) represent a double-degenerate symmetric O-Nb-O stretching vibration and a triply degenerate symmetric O-Nb-O bending vibration, respectively [24, 28]. Usually there are distinct shoulders in the Raman spectra on the low-frequency sides of the Raman mode at ~625 cm^{-1} in both orthorhombic and tetragonal phase, but the intensity of the tetragonal phase is weaker [29]. Furthermore, there is a broad weak peak in the 400–500 cm^{-1} regions, indicating the orthorhombic phase. As shown in Fig. 5, this characteristic shoulder in all Raman spectra is obviously visible. However, we observe a loss in Raman intensity in the 400–500 cm^{-1} regions. Its intensity becomes so weak that it is almost not observed for K$_x$NLN with x = 0.025. In contrast, the intensity in the 400–500 cm^{-1} regions is still visible for KN$_x$LN. The peaks around 625 cm^{-1} and 256 cm^{-1} obviously shift downward for overcompensated KNNLN by Na or K. This behavior is referred to a decrease in force constant caused by the change of length between Nb^{+5} and its coordinated oxygen in [BO$_6$] by pushing the B-site cation shifting away from the center of [BO$_6$]. This also implies that overcompensation of K or Na results in the formation of Nb^{+5} vacancies with negative charge. This can cause locally structural disorder and large lattice distortion, in order to maintain the charge balance [30, 31].

Figure 6(a)–(f) show the SEM images of the microstructure of thermally etched K$_x$NLN ceramics with $0.00 \leq x \leq 0.025$ sintered at 1080 °C for 3 h. In addition to the existence of pores and small size irregular grains, all ceramics consist of square-like or near square-like grains. The morphology of grain in all samples does not change significantly with increasing excess K. However, the appearance of abnormal grains can be observed when excess K content increases. It is reported [32, 33] that the liquid phase and a small amount of secondary phase, which melts at ~1000 °C, can form in KNN based ceramics due to the evaporation of Na. The liquid phases enhance sintering processing by accelerating particle rearrangment and atomic diffusion [34]. We believe the abnormal grain growth results from the liquid phases as well.

Fig. 6 SEM images of the fractured surface of K$_x$NLN ceramics with x = (**a**) 0, (**b**) 0.005, (**c**) 0.01, (**d**) 0.015, (**e**) 0.020, (**f**) 0.025
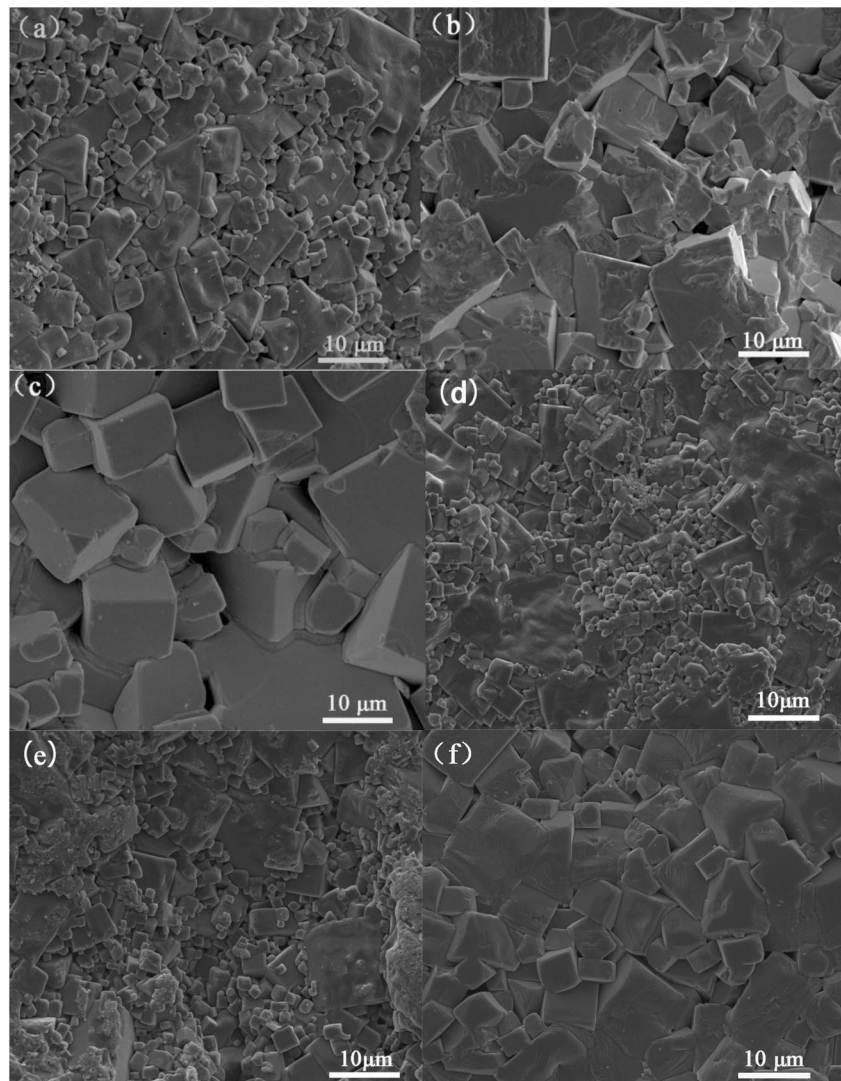
In contrast, it is interesting to observe that the microstructure evolution of KN$_y$LN is significantly different from that of K$_x$NLN. Figure 7(a)–(f) show the SEM images of the microstructure of thermally etched KN$_y$LN ceramics with $0.00 \leq y \leq 0.025$ sintered at 1050 °C for 3 h. There exist two stages in the microstructure evolution with increasing excess Na. The microstructure displaying abnormal grains surrounded by small grains in KN$_y$LN with $y \leq 0.005$ is similar to that of K$_x$NLN. It is expected since the small amount of excess Na is not enough to compensate the loss of Na. This can also promote the formation of Na-deficient liquid phase and subsequently abnormal grain growth. However, grain size of KN$_y$LN with $y \geq 0.01$ is much larger than that of K$_x$NLN. The grain size of KN$_y$LN with $y = 0.025$ reaches 8-10 μm. Another noticeable feature is that the grain size of KN$_y$LN is relatively homogeneous as compared with that of K$_x$NLN. The difference in the evolution of microstructure can be explained as follows. The addition of $y \geq 0.01$ excess Na is enough to compensate the loss of Na and then limit the formation of Na deficiency liquid phase. Although B-site vacancies are not common in perovskite ceramics [35], the overcompensation by either K or Na in KNLN can result in the presence of Nb^{+5} vacancies, which are considered to enhance mass transport during sintering. These observations leads us to conclude that the dominant mechanism of anormal grain growth in K$_x$NLN with $0.00 \leq x \leq 0.025$ and KN$_y$LN with $0.00 \leq y \leq 0.005$ is assisted by formation of liquid phase while coarsening of grains is assisted by presence of Nb^{+5} vacancies in KN$_y$LN with $0.01 \leq y \leq 0.025$.

Figure 8(a) and (b) show the temperature dependence of dielectric constant (ε_r) from room temperature to 160 °C on excess K and Na compensation, respectively. Two phase transition points are observed in all ceramics corresponding to the orthorhombic-tetragonal (OT-PTT) and cubic-tetragonal (T$_c$) phase transitions as shown as insets. Dielectric constant (ε_r), loss tangent, OT-PTT, T$_c$ (Curie temperature), and piezoelectric response d$_{33}$ for K$_x$NLN and KN$_y$LN ceramics are
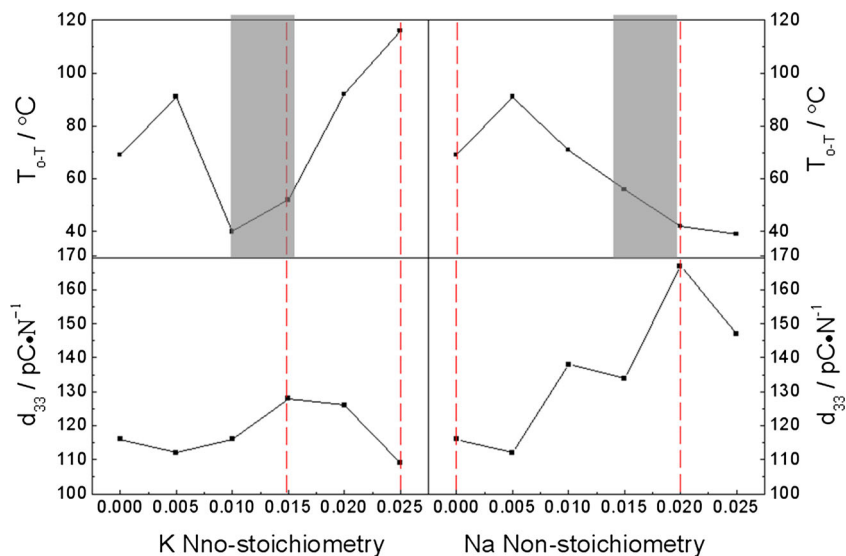

Fig. 7 SEM images of the fractured surface of KN$_y$LN ceramics with y = (**a**) 0, (**b**) 0.005, (**c**) 0.01, (**d**) 0.015, (**e**) 0.020, (**f**) 0.025
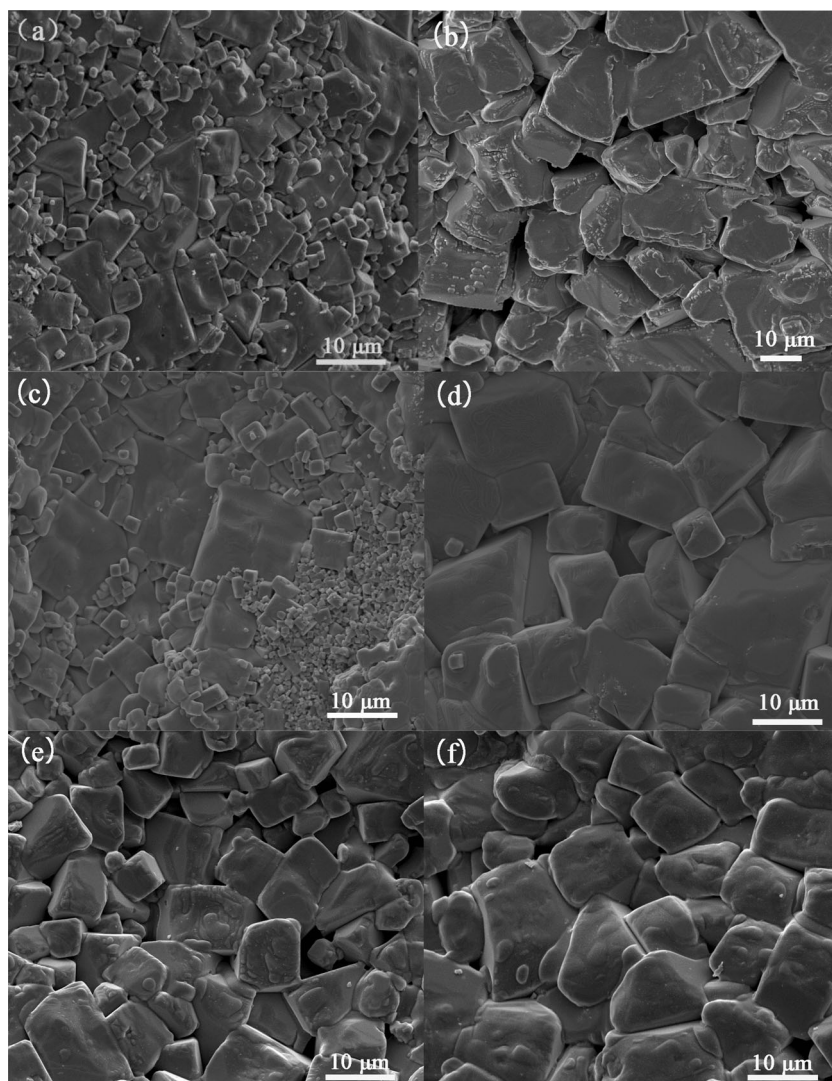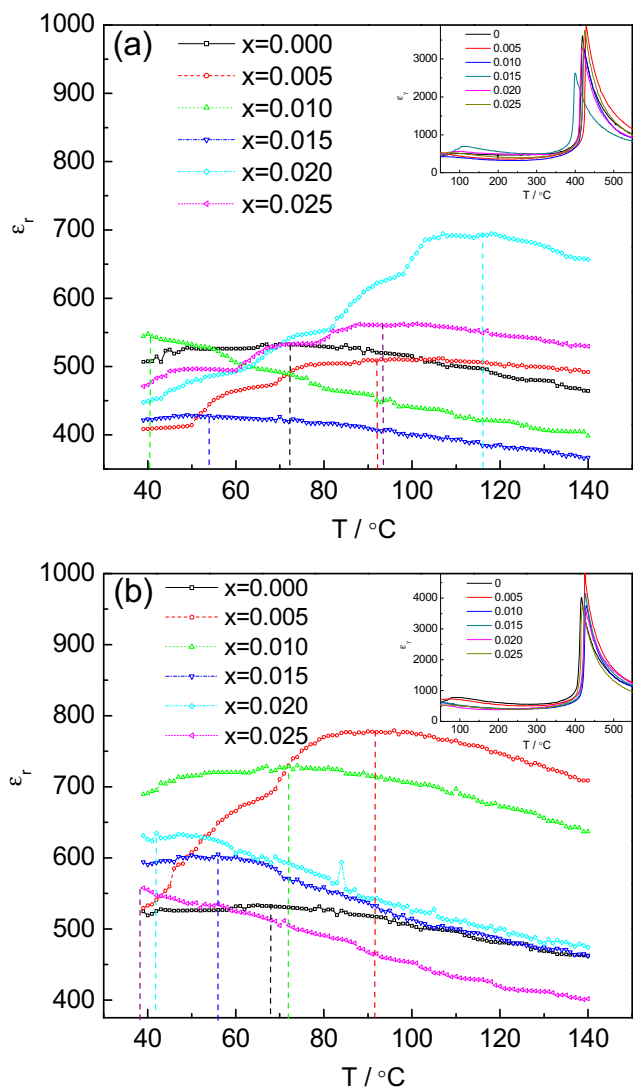
Fig. 8 Temperature dependence of ε_r for K_xNLN and KN_yLN ceramics with x, y = 0–0.025, measured from room temperature to 550 °C at 10 KHz

summarized in Table 1. As expected, there is no regular rule in the change of ε_r since the OT-PTT near around room temperature can result in the comparison of dielectric constants being complicated. Additionally, the dielectric constant is closely related to the grain size [36]. However, higher ε_r values usually lie in a narrow range in K_xNLN and KN_yLN ceramics with x = 0.010–0.015 and y = 0.010–0.020.

The dependence of OT-PTT and d_{33} on excess K and Na is further plotted in Fig. 9. As shown, the OT-PTT shows a trend of a shift to lower temperatures for KN_yLN ceramics with increasing excess Na until the actual stoichiometry is obtained. The lowest OT-PTT point appears between 40 °C and 52 °C for K_xNLN with x = 0.01–0.015, while the lowest OT-PTT point appears between 42 °C and 39 °C for KN_yLN with y = 0.02–0.025. Similar to the OT-PTT results, d_{33} values are very sensitive to a very small deviation from stoichiometry for both K_xNLN and KN_yLN ceramics as shown in Fig. 9. However, the dependence of OT-PPT and d_{33} is more significant for K_xNLN ceramics. When excess content of Na increases up to x = 0.02, a significantly enhanced d_{33} (~167 pC/N) is attained as compared with the d_{33} value (~116 pC/N) of uncompensated KNN ceramics. Further compensation of Na up to x = 0.025 results in a decrease of d_{33}. Overall, the samples with higher d_{33} and lower OT-PTT are usually achieved in K_xNLN ceramics with x = 0.010–0.015 and KN_yLN ceramics with x = 0.020–0.025. These observations imply that the compositions closest to stoichiometry are attained by compensating Na or K in a very narrow range of x = 0.010–0.015 or y = 0.020–0.025. These results are consistent with previous reports that the sodium evaporates more dramatically than the potassium at the same sintering temperature [33].

In a combination with results in Fig. 3, the close relationship between OT-PTT, d_{33}, and WRP of orthorhombic, tetragonal and monoclinic phase in K_xNLN and KN_yLN ceramics

Fig. 9 Dependence of OT-PTT and d_{33} on the content of (**a**) excess K and (**b**) excess Na. The shaded region represents compositions closest to the actual stoichiometry

emerges. A common trend noticed is that ceramics with the lower WRP of monoclinic phase present a lower OT-PTT point and a higher d_{33}. Our findings further confirm that an optimized weight ratio percentage exists in order to attain enhanced dielectric and electrical properties of KNN ceramics. It is also believed there is an optimum ratio between orthorhombic and tetragonal phase in these compositions. Subsequently, the OT-PPT shifts to near room temperature and the enhanced piezoelectric properties are attained for these ceramics.

It is important to point out that the amount of A-site nonstoichiometry is dependent on the sintering temperature. It has been shown [37, 38] that the optimum electrical properties can be attained by adjusting the sintering temperature. Wu et al. [39] reported enhanced piezoelectric properties were achieved in $K_{0.48}Na_{0.535}NbO_3$ when only excess A-site Na was added as well. Sung et al. [40] reported that the piezoelectric properties of $(Bi_{0.5}K_{0.5+x}Li_y)TiO_3$ ceramics by K nonstoichiometry and Li addition were significantly enhanced. We believe that these phenomena are actually ascribed to high sensitiveness of structures to A-site K or Na nonstoichiometry. However, it has been suggested that the dielectric properties can be significantly influenced by induced strain upon doping rather than chemical inhomogeneities and structural disorder, which are common occurrences in doped ferroelectrics [41]. It is clear that it is necessary to carry out further detailed phase structure study of KNN with slight deviation from stoichiometry.

4 Conclusions

The coexistence of three phases, orthorhombic, tetragonal, and monoclinic phases, in $0.94K_{0.5+x}Na_{0.5}NbO_3$–$0.06LiNbO_3$ and $0.94K_{0.5}Na_{0.5+y}NbO_3$–$0.06LiNbO_3$ lead-free ceramics (x, y = 0–0.025) at room temperature was observed. The weight ratio percentages of three phases along with the orthorhombic-tetragonal phase transition temperature and d_{33} were highly sensitive to A-site K or Na non-stoichiometry. Excess A-site Na played a dominant role in decreasing the weight ratio percentage of monoclinic phase and enhancing the electrical properties of KNN by shifting the orthorhombic-tetragonal phase transition temperature to around room temperature. As compared with uncompensated KNN ceramics of $d_{33} \sim 116pc/N$, significantly $d_{33} \sim 167pc/N$ was attained for $0.94K_{0.5}Na_{0.5+y}NbO_3$–$0.06LiNbO_3$ with y = 0.02.

References

1. A. J. Moulson, J. M. Herbert, *Electroceramics: materials, properties, applications*, Second edn. (John Wiley & Sons, West Sussex, 2003)
2. R. Guo, L. E. Cross, S. E. Park, B. Noheda, D. E. Cox, G. Shirane, Phys. Rev. Lett. **84**, 5423 (2000)
3. J. A. Perez, M. R. Soares, P. Q. Mantas, A. M. R. Senos, J. Eur. Ceram. Soc. **25**, 2207 (2005)
4. Y. Saito, H. Takao, T. Tani, T. Nonoyama, K. Takatori, T. Homma, T. Nagaya, M. Nakamura, Nature (London) **432**, 84 (2004)
5. M. R. Bafandeh, R. Gharahkhani, M. H. Abbasi, A. Saidi, J. S. Lee, H. S. Han, J. Electroceram. **33**, 128 (2014)
6. S. Swain, P. Kumar, J. Electroceram. **32**, 102 (2014)
7. G. Lévêque, P. Marchet, F. Levassort, L. P. Tran-Huu-Hue, J. R. Duclere, J. Eur. Ceram. Soc. **31**, 577 (2011)
8. R. López, F. González, M. E. Villafuerte-Castrejón, J. Eur. Ceram. Soc. **30**, 1549 (2010)
9. F. Rubio-Marcos, P. Ochoa, J. F. Fernandez, J. Eur. Ceram. Soc. **27**, 4125 (2007)
10. E. Hollenstein, M. Davis, D. Damjanovic, N. Setter, Appl. Phys. Lett. **87**, 182905 (2005)
11. F. Rubio-Marcos, M. G. Navarro-Rojero, J. J. Romero, P. Marchet, J. F. Fernández, IEEE Trans. Ultrason. Ferroelectr. Freq. Control **56**, 1835 (2009)
12. Y. J. Dai, X. W. Zhang, K. P. Chen, Appl. Phys. Lett. **94**, 042905 (2009)
13. Y. Guo, K. I. Kakimoto, H. Ohsato, Appl. Phys. Lett. **85**, 4121 (2004)
14. Y. H. Lee, J. H. Cho, B. I. Kim, D. K. Choi, J. Appl. Phys. **47**, 4620 (2008)
15. L. Zheng, J. Wang, J. Electroceram. **32**, 192 (2014)
16. C. Miclea, C. Tanasoiu, C. F. Miclea, L. Amarande, A. Gheorghiu, I. Spanulescu, C. Plavitu, C. T. Miclea, M. C. Cioangher, L. Trupina, A. Iuga, J. Eur. Ceram. Soc. **27**, 4055 (2007)
17. M. S. Kim, D. S. Lee, E. C. Park, S. J. Jeong, J. S. Song, J. Eur. Ceram. Soc. **27**, 4121 (2007)
18. J. G. Wu, D. Q. Xiao, Y. Y. Wang, J. G. Zhu, L. Wu, Y. H. Jiang, Appl. Phys. Lett. **91**, 252907–252909 (2007)
19. P. Zhao, B. P. Zhang, J. F. Li, Scripta Mater. **58**, 429 (2008)
20. D. M. Lin, K. W. Kwok, H. L. Chan, J. Am. Ceram. Soc. **92**, 2765 (2009)
21. N. Zhang, A. M. Glazer, D. Baker, P. A. Thomas, Acta Crystallogr. Sect. B: Struct. Sci. **65**, 291 (2009)
22. S. J. Liu, B. B. Wan, P. F. Wang, S. H. Song, Scripta Mater. **63**, 124 (2010)
23. F. Rubio-Marcos, P. Marchet, T. Merle-Méjean, J. F. Fernández, Mater. Chem. Phys. **123**, 91 (2010)
24. N. Klein, E. Hollenstein, D. Damjanovic, H. J. Trodahl, N. Setter, M. Kuball, J. Appl. Phys. **102**, 014112 (2007)
25. T. A. Skidmore, T. P. Comyn, S. J. Milne, Appl. Phys. Lett. **94**, 222902 (2009)
26. D. W. Baker, P. A. Thomas, N. Zhang, A. M. Glazer, Appl. Phys. Lett. **95**, 091903 (2009)
27. D. W. Baker, P. A. Thomas, N. Zhang, A. M. Glazer, Acta Crystallogr. Sect. B: Struct. Sci. **65**, 22 (2009)
28. F. Rubio-Marcos, M. A. Bañares, J. J. Romero, J. F. Fernández, J. Raman Spectrosc. **42**, 639 (2011)
29. H. J. Trodahl, N. Klein, D. Damjanovic, N. Setter, B. Ludbrook, D. Rytz, M. Kuball, Appl. Phys. Lett. **93**, 262901 (2008)
30. R. J. C. Lima, W. Paraguassu, P. T. C. Freire, J. M. Sasaki, F. E. A. Melo, J. Mendes Filho, S. Lanfredi, J. Raman Spectrosc. **42**, 639 (2011)
31. H. R. Xia, H. C. Chen, H. Yu, K. X. Wang, B. Y. Zhao, Phys. Stat. Sol. (b) **210**, 47 (1998)

32. K. H. Cho, H. Y. Park, C. W. Ahn, S. Nahm, J. Am. Ceram. Soc. **90**, 1946 (2007)
33. Y. H. Zhen, J. F. Li, J. Am. Ceram. Soc. **90**, 3496 (2007)
34. L. J. Cheng, L. Liu, Q. Ma, S. J. Liu, Scripta Mater. **111**, 102 (2016)
35. K. H. Härdtl, D. Hennings, J. Am. Ceram. Soc. **55**, 230 (1972)
36. S. J. Liu, V. Zenou, I. Sus, T. Kotani, M. Schilfgaarde, N. Newman, Acta Mater. **55**, 2647 (2007)
37. P. Zhao, B. P. Zhang, J. F. Li, J. Am. Ceram. Soc. **91**, 1690 (2008)
38. P. Zhao, B. P. Zhang, J. F. Li, Appl. Phys. Lett. **90**, 242909 (2007)
39. J. G. Wu, D. Q. Xiao, Y. Y. Wang, L. Wu, Y. H. Jiang, J. G. Zhu, J. Am. Ceram. Soc. **91**, 2385 (2008)
40. Y. S. Sung, H. M. Lee, W. Du, H. G. Yeo, S. C. Lee, J. H. Cho, T. K. Song, M. H. Kim, Appl. Phys. Lett. **94**, 062901 (2009)
41. K. Datta, K. Roleder, P. A. Thomas, Phys. Rev. B **82**, 224105 (2010)